

Single and double finger-gate controlled spin electronic transport with an in-plane magnetic field

Chi-Shung Tang,^{1,*} Jia-An Keng,¹ Nzar Rauf Abdullah,² and Vidar Gudmundsson³

¹*Department of Mechanical Engineering, National United University, Miaoli 36063, Taiwan*

²*Physics Department, College of Science, University of Sulaimani, Kurdistan Region, Iraq*

³*Science Institute, University of Iceland, Dunhaga 3, IS-107 Reykjavik, Iceland*

A propagation matrix method is proposed to investigate spin-resolved electronic transport in single finger-gate (SFG) and double finger-gate (DFG) controlled split-gate quantum devices. We show how the interplay of the Rashba and Dresselhaus spin-orbit (SO) interactions as well as a Zeeman (Z) field influences the quantum transport characteristics. Without the Dresselhaus effect, the conductance reveals a mirror symmetry between the hole-like and the electron-like quasi-bound states in the SO-Z gap energy regime in the SFG system, but not for the DFG system. For the Dresselhaus interaction, we are able to analytically identify the binding energy of the SFG and DFG bound states. Furthermore, the DFG resonant states can be determined by tuning the distance between the finger gates.

PACS numbers: 73.23.-b, 72.25.Dc, 72.30.+q

I. INTRODUCTION

Spintronics utilizing the spin degree of freedom of conduction electrons is an emerging field of research due to its applications from logic to storage devices with low power consumption.¹⁻³ Manipulating the spin information offers the possibility to scale down devices to the nanoscale and is favorable for applications in quantum computing.⁴⁻⁶

Structure inversion asymmetry (SIA) originates from the inversion asymmetry of the confining potential and yields the Rashba SO coupling term in the Hamiltonian H_R , whose strength can be manipulated by an external field.⁷ SO interaction allows for coupling of electron spin and orbital degrees of freedom without the action of a magnetic field.^{8,9} The Rashba SO coupling is of importance in the study of spintronic devices in semiconductor materials with two-dimensional electron gases (2DEG).¹⁰⁻¹³

Experimentally, the Rashba interaction has been shown to be effective for electron spin manipulation by using bias-controlled gate contacts.¹⁵ Recently, several approaches were proposed to engineer a spin-resolved subband structure utilizing magnetic fields¹⁶⁻²¹ or ferromagnetic materials.^{22,23} The combination of a Rashba SO coupling and an external in-plane magnetic field may modify the subband structure producing a spin-split Rashba-Zeeman (RZ) subband gap feature.^{24,25} To implement a quantum information storing and transfer, not only coherent manipulation, but also resonant features involving SO couplings are of importance.²⁶ This can be achieved utilizing a double finger gate (DFG) forming a quantum dot in between the fingers where electrons are subjected to the Rashba SO coupling and the Zeeman interaction.

Because of the bulk inversion asymmetry (BIA) in III-V semiconducting materials, the Dresselhaus SO coupling²⁷ may be induced involving \mathbf{k} -linear and \mathbf{k} -cubic

contributions, given by the Hamiltonian

$$H_D = \beta (\sigma_x k_x - \sigma_y k_y) + \gamma (-\sigma_x k_x k_y^2 + \sigma_y k_y k_x^2) \quad (1)$$

where the strength of the linear in \mathbf{k} term $\beta = \gamma \langle k_z^2 \rangle$ stems from crystal fields. These SO coupling terms in semiconductor layers are described by the Hamiltonian $H_{SO} = H_R + H_D$.

In this work, we consider a finger-gate (FG) controlled narrow constriction^{28,29} in the presence of a RZ subband gap, in which a very asymmetric structure in the 2DEG leads to strong SO coupling with the result that the Rashba effect is dominant. The Dresselhaus effect due to BIA is also considered. Below, the SFG and DFG controlled spin-resolved electronic transport properties will be compared in an external in-plane magnetic field as shown in Fig. 1.

The organization of the rest of this paper is as follows. In Sec. II we describe the propagation-matrix approach of tunneling through a DFG system under in-plane magnetic field. In Sec. III we present our calculated results on the spin-split subband structure and the spin-resolved conductance. A concluding remarks is given in Sec. IV.

II. SPIN ELECTRONIC TRANSPORT MODEL

In this section, we show that the RZ and RD-Z effects, described by a Hamiltonian technique lead to, respectively, symmetric and asymmetric spin-split subband structures. In addition, the SFG and DFG influence on the transport through the SG confined quantum channel will be described by a spin-dependent PM method.

As is illustrated for the device in Fig. 1, a two dimensional electron gas (2DEG) is induced in an InAs-In_{1-x}Ga_xAs semiconductor heterojunction grown in the (001) crystallographic direction and is subjected to a split-gate voltage. A pair of split-gates restricts the movement of the electrons of the 2DEG, and therefore

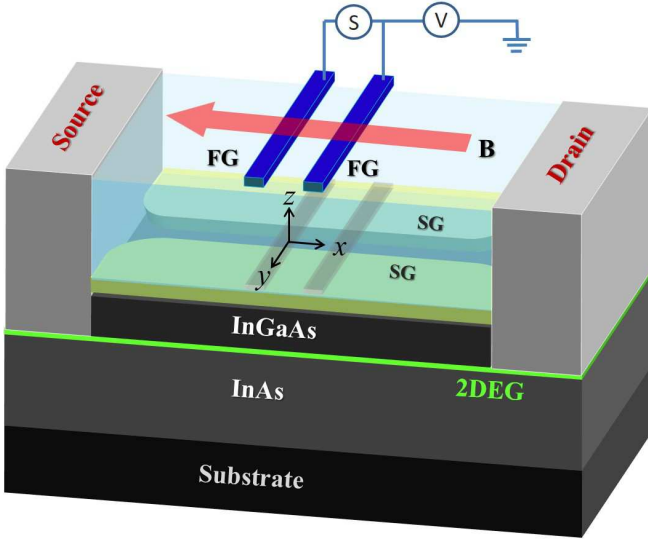


FIG. 1. (Color online) Schematic of the SFG and DFG devices controlled by a switch (S) and a gate potential V . A split-gate is used to control the channel width. An external in-plane magnetic field $\mathbf{B} = B\hat{x}$ ($B < 0$) is applied. The DFG is consisted of two finger gates located x_1 and x_2 to influence the spin-resolved resonant quantum transport.

a quantum channel is generated in the $[100]$ direction. Propagating electrons in the channel are driven from source to drain.

In the absence of the finger gates, a transported electron is affected by the Rashba effect H_R due to SIA and the Zeeman effect H_Z induced by an external in-plane magnetic field, described by the unperturbed Hamiltonian

$$\tilde{H}_0 = H_0 + H_R + H_D + H_Z. \quad (2)$$

The first term describes a bare quantum channel that is described by the ideal Hamiltonian

$$H_0 = \frac{\hbar^2 k^2}{2m^*} + U_{SG}(y). \quad (3)$$

The first term is the kinetic energy of an electron in the 2DEG, where $\hbar = h/2\pi$ is the reduced Planck constant. A conduction electron has an assigned wave number k satisfying $k^2 = k_x^2 + k_y^2$ and m^* is its effective mass. The second term indicates a split-gate induced confining potential energy that can be modeled by a hard-wall confinement with width W for simplicity.

In the second term of Eq. (2), we consider a (001) crystallographic 2DEG system, and hence the Rashba SO Hamiltonian $H_R = \alpha(\boldsymbol{\sigma} \times \mathbf{k}) \cdot \hat{z}$ coupling the Pauli spin matrix $\boldsymbol{\sigma}$ to the momentum $\mathbf{p} = \hbar\mathbf{k}$ can be reduced to a k -linear form

$$H_R = \alpha(\sigma_x k_y - \sigma_y k_x), \quad (4)$$

$$H_D = \beta(\sigma_x k_x - \sigma_y k_y), \quad (5)$$

where the Rashba coupling strength α is proportional to the electric field along the \hat{z} direction perpendicular to the 2DEG.¹⁵ The fourth term in Eq. (2) describes an applied external in-plane magnetic field that is selected to be antiparallel to the channel in the $[100]$ direction and has the form $\mathbf{B} = B\hat{x}$ ($B < 0$). The longitudinal in-plane magnetic field induces a Zeeman term that can be expressed as

$$H_Z = g\mu_B B\sigma_x, \quad (6)$$

in which $g = g_s/2$ indicates half of the effective gyromagnetic factor ($g_s = -15$ for InAs) and $\mu_B = 5.788 \times 10^{-2}$ meV/T is the Bohr magneton.

Tuning the switch shown in Fig. 1 allows us to investigate SFG and DFG controlled spin-resolved transport properties. We consider the width of the finger-gate scattering potential, W , to be less than the Fermi wave length $\lambda_F = 31.4$ nm and to be described by a delta potential. In addition, we assume a high-mobility semiconductor materials so that impurity effects can be neglected. A FG array system can generally be described by the scattering potential energy

$$U_{FG}(x) = \sum_{j=1}^{N_{FG}} U_j \delta(x - x_j), \quad (7)$$

where U_j indicates a delta potential energy induced by the FG j , and N_{FG} is the number of FG. For example, $N_{FG} = 1$ and 2 indicate, respectively, SFG or DFG systems. These FG array systems under the influence of the RD-Z effects can be formally described by the Schrödinger equation

$$[\tilde{H}_0 + U_{FG}(x)] \Psi(x, y) = E\Psi(x, y). \quad (8)$$

The eigenfunction $\Psi(x, y)$ in Eq. (8) can be obtained by summing over all occupied subbands, n , for the product of the spatial wave functions and the spin states, given by

$$\Psi(x, y) = \sum_n \phi_n(y) e^{ik_x x} \chi_n. \quad (9)$$

Here the ideal transverse wave function in subband n is $\phi_n(y) = (2/W)^{1/2} \sin(k_n y)$, in which the subband energy $\varepsilon_n = \hbar^2 k_n^2 / 2m^*$ with the quantized wave number $k_n = n\pi/W$.

For simplicity, we employ the Fermi-level in a 2DEG as an energy unit, namely $E^* = E_F = \hbar^2 k_F^2 / 2m^*$ with m^* and \hbar being, respectively, the effective mass of an electron and the reduced Planck constant. In addition, one selects the inverse wave number as a length unit, namely $l^* = k_F^{-1}$. Correspondingly, the magnetic field is in units of $B^* = \mu_B^{-1} E^*$, and the Rashba SO-coupling constant α is in units of $\alpha^* = 2E^* l^*$. In the following we consider a sufficient narrow channel by assuming the channel width $W = \pi l^* = 15.7$ nm so that the bare

subband energy is simply $\varepsilon_n = n^2$. The energy dispersion can thus be expressed as

$$E_n^\sigma(k_x) = \varepsilon_n + k_x^2 + \sigma \sqrt{(2\beta k_x + gB)^2 + (2\alpha k_x)^2}, \quad (10)$$

where $\sigma = \pm$ indicates the upper (+) and lower (−) spin branches. Sufficiently low temperature $k_B T < 0.1\Delta\varepsilon$ or $T < 23$ K is required to avoid thermal broadening effects.

In order to investigate the SFG and DFG controlled spin-resolved electronic transport properties, we shall explore how the spin-mixing effect due to the interplay of the RD-Z effects influences the propagating and evanescent modes. For a given incident electron energy $E_n = E - \varepsilon_n$ in the subband n , the energy dispersion is related to complex wave number that obeys

$$k_x^4 - [4(\alpha^2 + \beta^2) + 2E_n] k_x^2 - 4gB\beta k_x + [E_n^2 - (gB)^2] = 0. \quad (11)$$

To proceed, one has to label the four longitudinal wave numbers k_x as the right-going k^σ and left-going q^σ , in which the notation $\sigma = +$ indicates spin-up mode and $\sigma = -$ stands for spin-down mode.

Below, we focus on a sufficiently narrow quantum channel to explore the first two conductance steps associated with the two spin branches of a transported electron occupying the lowest subband. We calculate the quantum transport properties by using a generalized PM method, in which the spin-flip scattering mechanisms is taken into account. The energy dispersion shown in Fig. 2(a) essentially divides the energy spectrum into three regimes, namely the low energy regime $E_{0R}^- < E < E_{0T}^-$, the intermediate energy regime $E_{0T}^- < E < E_0^+$, and the high energy regime $E > E_0^+$. In the low and high energy regimes, there are four propagating modes with real k_σ and real q_σ . It should be noted that there are two propagating and two evanescent modes in the intermediate energy regime or the RZ energy gap region where the evanescent modes manifest a bubble behavior with imaginary wave vectors.²⁸

The spin-split wave functions around the scattering potential U_{FG} located at x_j can be formally expressed including the spatial and spin parts as

$$\begin{aligned} \psi_{j-1}(x) = & \sum_{\sigma=\pm} \sum_{\sigma'=\sigma,\bar{\sigma}} \left\{ A_{j-1}^{\sigma,\sigma'} e^{ik^{\sigma'}(x-x_j)} \begin{bmatrix} a^{\sigma'} \\ b^{\sigma'} \end{bmatrix} \right. \\ & \left. + B_{j-1}^{\sigma,\sigma'} e^{iq^{\sigma'}(x-x_j)} \begin{bmatrix} c^{\sigma'} \\ d^{\sigma'} \end{bmatrix} \right\}, \quad x < x_j \end{aligned} \quad (12)$$

and

$$\begin{aligned} \psi_j(x) = & \sum_{\sigma=\pm} \sum_{\sigma'=\sigma,\bar{\sigma}} \left\{ C_j^{\sigma,\sigma'} e^{ik^{\sigma'}(x-x_j)} \begin{bmatrix} a^{\sigma'} \\ b^{\sigma'} \end{bmatrix} \right. \\ & \left. + D_j^{\sigma,\sigma'} e^{iq^{\sigma'}(x-x_j)} \begin{bmatrix} c^{\sigma'} \\ d^{\sigma'} \end{bmatrix} \right\}, \quad x > x_j \end{aligned} \quad (13)$$

where $A_{j-1}^{\sigma,\sigma'}$ and $C_j^{\sigma,\sigma'}$ indicate the coefficients of right-going electrons with positive group velocity and wave

number k^σ , while $B_{j-1}^{\sigma,\sigma'}$ and $D_j^{\sigma,\sigma'}$ stand for the coefficients of the left-going electrons with negative group velocity and wave number q^σ . There are two boundary conditions around x_j , given by

$$\psi_{j-1}(x_j^-) = \psi_j(x_j^+), \quad (14a)$$

$$\psi'_{j-1}(x_j^-) = \psi'_j(x_j^+) - U_j \psi_j(x_j^+). \quad (14b)$$

Taking into account the possible incident spin states σ and $\bar{\sigma}$ allows us to formulate the total PM \mathbf{P} in an arbitrary FG array system.

$$\begin{bmatrix} \mathbf{1} \\ \mathbf{r} \end{bmatrix} = \mathbf{P} \begin{bmatrix} \mathbf{t} \\ \mathbf{0} \end{bmatrix}, \quad (15)$$

or expressed explicitly

$$\begin{bmatrix} 1 & 0 \\ 0 & 1 \\ r_{\sigma,\sigma} & r_{\bar{\sigma},\sigma} \\ r_{\sigma,\bar{\sigma}} & r_{\bar{\sigma},\bar{\sigma}} \end{bmatrix} = \mathbf{P} \begin{bmatrix} t_{\sigma,\sigma} & t_{\bar{\sigma},\sigma} \\ t_{\sigma,\bar{\sigma}} & t_{\bar{\sigma},\bar{\sigma}} \\ 0 & 0 \\ 0 & 0 \end{bmatrix}. \quad (16)$$

Here, the diagonal and off-diagonal terms in \mathbf{r} and \mathbf{t} indicate, respectively, the spin-preserve (SP) and spin-flip (SF) reflection and transmission coefficients. The first subscript is the incident spin state, and the second one is the scattered spin state.

To proceed, one has to consider both the σ and $\bar{\sigma}$ spin states incident from the source electrode. The PM for the electrons with two spin states in the j -th region can be expressed as $\mathbf{p}_j = \mathbf{p}_{j,\delta} \mathbf{p}_{j,\text{free}}$, in which $\mathbf{p}_{j,\delta}$ is the PM through the FG j and $\mathbf{p}_{j,\text{free}}$ is the free space PM between the FG j and $j+1$. Hence, the total PM for SFG and DFG can be simply expressed as $\mathbf{P}_{\text{SFG}} = \mathbf{p}_1$ and $\mathbf{P}_{\text{DFG}} = \mathbf{p}_1 \mathbf{p}_2$. In addition, $\mathbf{p}_{j,\text{free}}(i, j) = \exp(-ik_{i,j}L)$ if $i = j$, or identically zero if $i \neq j$, in which $k_{1,1} = k^\sigma$ and $k_{2,2} = k^{\bar{\sigma}}$ are right-going wave vectors, while $k_{3,3} = q^\sigma$ and $k_{4,4} = q^{\bar{\sigma}}$ are left-going wave numbers. Solving the PM equation numerically, we may obtain the reflection and transmission coefficients of the scattered intermediate and final states through the SFG or DFG systems.

We consider an electron injected from the left reservoir (source electrode) and transported to the right reservoir (drain electrode) for a given incident energy. Solving for the spin non-flip and flip reflection coefficients $r_{\sigma,\sigma}$ and $r_{\sigma,\bar{\sigma}}$, as well as the spin non-flip and flip transmission coefficients $t_{\sigma,\sigma}$ and $t_{\sigma,\bar{\sigma}}$, we can calculate numerically the conductance based on the Landauer-Büttiker framework^{30,31}

$$G = g_0 \sum_{\sigma_L, \sigma_R} \frac{v_{\sigma_R}}{v_{\sigma_L}} |t_{\sigma_L, \sigma_R}|^2. \quad (17)$$

Here $g_0 = e^2/h = 25.8 \text{ k}\Omega^{-1}$ is the conductance quantum per spin state, and σ_L and σ_R indicate, respectively, the spin branches of the incident and transmitted waves in the left and right leads. Therefore, v_{σ_L} and v_{σ_R} represent the group velocity of corresponding modes in the left and right reservoirs, respectively.

III. NUMERICAL RESULTS

Calculations presented below are carried out under the assumption of a 2DEG at a high-mobility InAs-In_{1-x}Ga_xAs semiconductor interface with an electron effective mass $m^* = 0.023m_0$ and typical electron density $n_e \sim 10^{12} \text{ cm}^{-2}$.¹⁵ Accordingly, the energy unit is $E^* = 66 \text{ meV}$, the length unit $l^* = 5.0 \text{ nm}$, the magnetic field unit $B^* = 1.14 \text{ kT}$, and the spin-orbit coupling parameter is in units of $\alpha^* = 330 \text{ meV}\cdot\text{nm}$. In addition, we assume that the width of the finger gate is $l_{\text{FG}} = l^*$ such that the FG potential energy $V_j = U_j/l_{\text{FG}}$ is in units of $V^* = 66 \text{ meV}$. Below, we assume that $V_1 = V_2 = V$ for simplicity. By using the above units, all physical quantities presented below are dimensionless.²⁸

Our previous work has demonstrated that the interplay of the SO interaction and the Zeeman effect may generate a SO-Z gap due to the orthogonality of the SO effective magnetic field and the in-plane magnetic field.¹⁴ In Fig. 2, we show the energy spectrum of the lowest subband. The chosen parameters correspond to a strong SO coupling regime with SO-Z gap. The transported spin-resolved electrons can thus be separated into the low-energy ($E_{0R}^- < E < E_{0T}^-$), the SO-gap ($E_{0T}^- < E < E_{0T}^+$), and the high-energy ($E_{0T}^+ < E$) regimes. Figure 2(a)-(b) indicates two spin-state energies for a given wave number obtained from Eq. (10), while Figure 2(c)-(d) displays four complex wave numbers for a given electron energy obtained from Eq. (11).

Concerning the Rashba-Zeeman (RZ) effect, Fig. 2(a) shows that the subband bottom energy of the spin-up branch is at $E_0^+ = \varepsilon_1 + gB = 1.02$, and the subband top energy of the spin-down branch is $E_{0T}^- = \varepsilon_1 - gB = 0.98$. Hence, the RZ gap $\Delta E_{\text{RZ}} = E_0^+ - E_{0T}^- = 2gB = 0.04$. This is exactly the Zeeman gap ΔE_Z . In addition, the left and right spin-down subband bottoms are at the same energy, namely $E_{0L}^- = E_{0R}^- = 0.9575$.

Concerning the Rashba-Dresselhaus-Zeeman (RDZ) effect ($\beta = 0.1$), Fig. 2(b) shows that spin-up subband bottom becomes slightly lower ($E_0^+ = 1.018$), and the spin-down subband top becomes slightly higher ($E_{0T}^- = 0.982$). Hence, the RDZ gap $\Delta E_{\text{RDZ}} = 0.036$ is smaller than the RZ gap ΔE_{RZ} by 0.004. Moreover, the left and right spin-down subband bottoms are no longer the same, that is, $E_{0L}^- = 0.9571$ and $E_{0R}^- = 0.9395$. Below, we shall show that these asymmetric subband bottoms may lead to interesting transport properties.

In order to explore the spin-resolved transport properties, it is important to define the group velocity of an electron in the σ spin branch

$$v^\sigma(k_x) = 2k_x + \sigma \frac{4(\alpha^2 + \beta^2)k_x + 2\beta gB}{\sqrt{(2\alpha k_x)^2 + (2\beta k_x + gB)^2}}. \quad (18)$$

Defining the velocity allows us to determine a local minimum and a maximum in the subband structures by setting the group velocity identically zero.

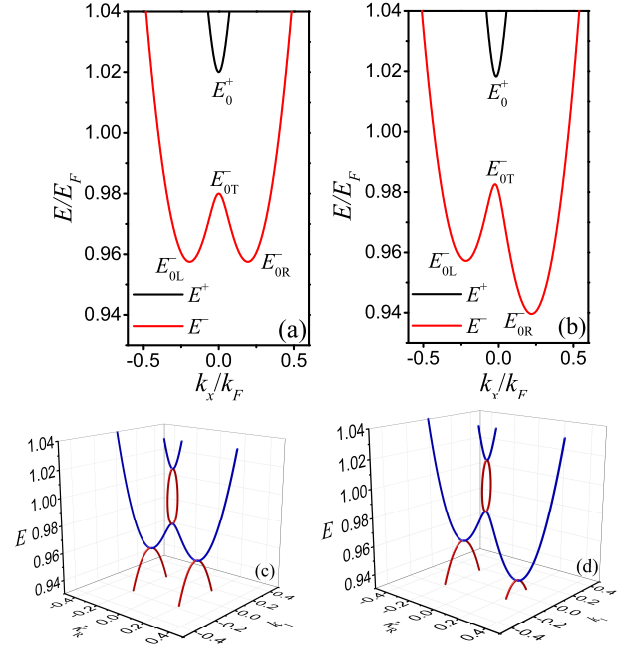


FIG. 2. (Color online) (a)-(b) Energy spectrum as a function of real wave number; (c)-(d) propagating (blue) and evanescent (red) modes versus complex wave number $k = k_R + ik_I$. The Dresselhaus coefficients are $\beta = 0.0$ for (a) and (c); $\beta = 0.1$ for (b) and (d). The other parameters are $\alpha = 0.2$, $gB = 0.02$.

Without the Dresselhaus effect, the two subband bottoms in the lower spin branch can be analytically obtained at $k_x = \pm [\alpha^2 - (gB/2\alpha)^2]^{1/2}$ corresponding to the same subband bottom energy $E_{0L}^- = E_{0R}^- = 1 - [\alpha^2 + (gB/2\alpha)^2]$. With the Dresselhaus effect, this degeneracy subband bottom will be broken as is shown in Fig. 2(b). Fig. 2(c) and (d) show their corresponding energy dispersion with respect to complex k_x that is important to perform transport calculation.

In Fig. 3, we compare the conductance behavior of SFG and DFG systems with no Dresselhaus effect. The conductance in the SFG system shown in Fig. 3 (a) and (b) reveals a perfect mirror effect between the electron-like QBS (EQBS) for negative V and hole-like QBS (HQBS) for positive V . Moreover, the QBS dips for $V = \pm 0.2$ become the QBS valleys for $V = \pm 0.6$. This indicates that a stronger voltage results in a shorter QBS life time.

It is interesting to compare the SFG with voltage V to a DFG with voltage $V/2$ and keep the two FGs very close, say with $L = 10$, as shown in Fig. 3 (c) and (d). It is surprising that the EQBS structures in the DFG and the SFG system at a negative V are almost unchanged, but the HQBS structures are very different. Fig. 3(c) demonstrates that a weak positive voltage ($V = 0.1$) in the DFG system does not allow a formation of a HQBS. If the voltage is increased to 0.3, the HQBS valley in SFG becomes a dip around E_{0T}^- and a Fano dip in the SO-Z

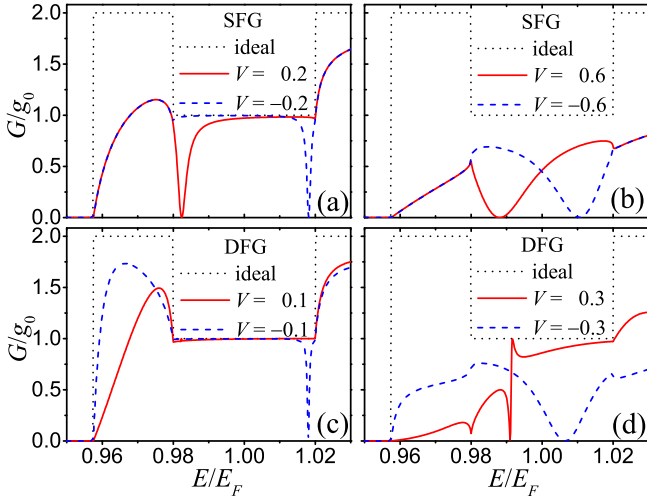


FIG. 3. (Color online) Conductance as a function of energy in the absence of Dresselhaus effect for (a)-(b) SFG system, in comparison with (c)-(d) DFG system with $L = 10$. $\alpha = 0.2$, $\beta = 0.0$, and $gB = 0.02$.

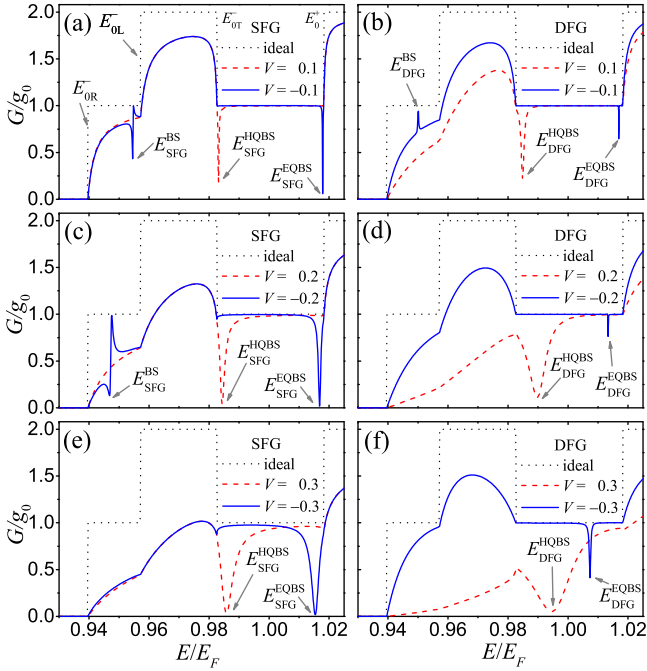


FIG. 4. (Color online) Conductance as a function of energy in the presence of Dresselhaus effect for SFG system in comparison with DFG system with $L = 5$. $\alpha = 0.2$, $\beta = 0.1$, and $gB = 0.02$

gap as shown in Fig. 3(d).

In Fig. 4, we show the conductance of SFG and DFG systems as a function of electronic energy in the presence of Dresselhaus SO interaction ($\beta = 0.1$) for $V =$ (a)-(b) ± 0.1 ; (c)-(d) ± 0.2 ; and (e)-(f) ± 0.3 . The other parameters $\alpha = 0.2$ and $gB = 0.02$, satisfying $\alpha^2 + \beta^2 > gB$,

are within the strong SO coupling regime.

In the case of a SFG, sufficient low energy $E < E_{0L}^-$ with negative FG voltage may result in a Fano line-shape (see Fig. 4(a) and (c)). This is due to the interference between the SFG BS $E_{\text{SFG}}^{\text{BS}}$ below the left spin-down bottom and the extended state at the right spin-down branch. The binding energy of the SFG BS can be analytically predicted to be $E_{\text{SFG}}^b = V^2/4 = 0.0025$ ($V = -0.1$) and 0.01 ($V = -0.2$), as shown by solid blue lines. This binding energy can also be numerically determined using

$$E_{\text{SFG}}^b = E_{0L}^- - E_{\text{SFG}}^{\text{BS}} \quad (19)$$

with $E_{0L}^- = 0.957$, while $E_{\text{SFG}}^{\text{BS}} = 0.9545$ ($V = -0.1$) and 0.9468 ($V = -0.2$). We thus numerically obtain the SFG BS binding energy $E_{\text{SFG}}^b = 0.0026$ ($V = -0.1$) and 0.0103 ($V = -0.2$) that is approximately the same as our analytical prediction delivers.

If the incident electron energy is within the gap region, the mirror effect between the HQBS and EQBS is clearly shown in the SFG system. More precisely, the SFG HQBS energies $E_{\text{SFG}}^{\text{HQBS}} = 0.9831, 0.9843, 0.9857$ for $V = 0.1, 0.2, 0.3$, respectively, are slightly above the spin-down top energy $E_{0T}^- = 0.982$. Accordingly, the SFG EQBS energies $E_{\text{SFG}}^{\text{EQBS}} = 1.0178, 1.0168, 1.0153$ for $V = -0.1, -0.2, -0.3$, respectively, are slightly below the spin-up bottom energy $E_0^+ = 1.018$. The higher $|V|$ may slightly shift the HQBS and EQBS toward the center of the SO-Z gap.

In the case of a DFG shown in Fig. 4, a sufficient low energy $E < E_{0L}^- = 0.957$ with a negative FG potential $V = -0.1$ may result in a sharp peak (see Fig. 4(b)) corresponding to a DFG BS energy $E_{\text{DFG}}^{\text{BS}} = 0.9501$ below E_{0L}^- . The DFG BS binding energy can be numerically obtained

$$E_{\text{DFG}}^b = E_{0L}^- - E_{\text{DFG}}^{\text{BS}} \quad (20)$$

giving $E_{\text{DFG}}^b = 0.0069$ in units of E_F .

In order to provide an evidence of such a DFG BS mechanism, we derive an analytical expression for E_{DFG}^b , given by

$$\frac{|V|}{\sqrt{E_{\text{DFG}}^b}} - 1 = \tanh\left(\sqrt{E_{\text{DFG}}^b} \frac{L}{2}\right). \quad (21)$$

This equation allows us to analytically estimate the binding energy $E_{\text{DFG}}^b = 0.00689$ for $V = -0.1$ and $L = 5$. This is only a bit smaller than our numerical result.

Comparing Figs. 4(b), (d), and (f), we see that if the DFG potential is negatively increased, the electron-like QBS (EQBS) dip is red shifted towards the center of the SO-Z gap and becomes more significant. If $V = -0.2$, as is shown in Fig. 4(d), the DFG binding energy $E_{\text{DFG}}^b = 0.02$ as can be estimated from Eq. (21), the corresponding BS energy $E_{\text{DFG}}^{\text{BS}} = 0.937$ is below the subband threshold E_{0R}^- . The DFG BS thus disappears in Fig. 4(d) as well as Fig. 4(f). On the contrary, increasing the positive DFG

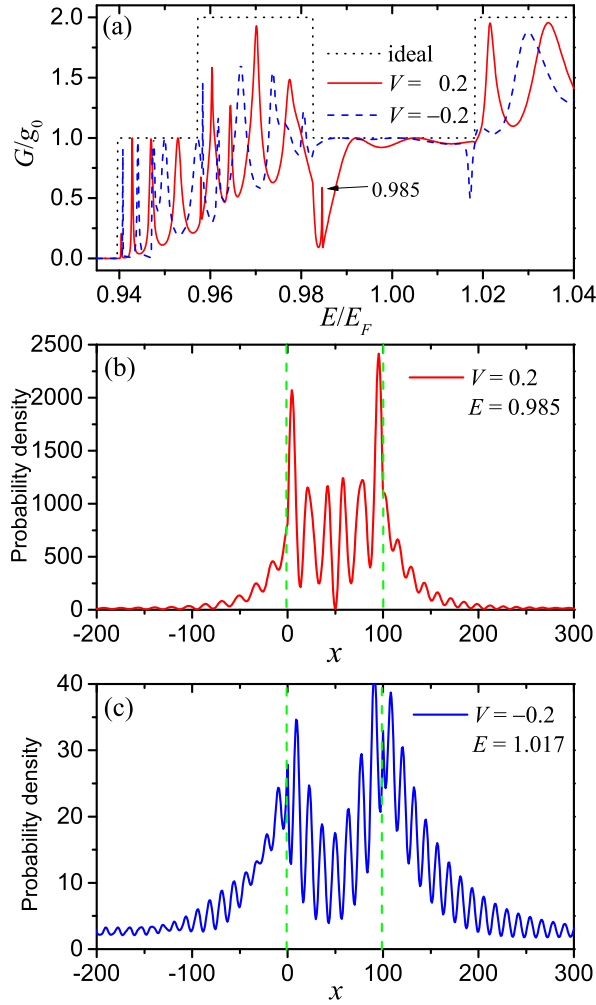


FIG. 5. (Color online) (a) Conductance as a function of energy for DFG system with $L = 100$ (500 nm). The corresponding probability densities are shown in (b) $V = 0.2$, $E = 0.985$; and (c) $V = -0.2$, $E = 1.017$. Other parameters are $\alpha = 0.2$, $\beta = 0.1$, and $gB = 0.02$

potential ($V > 0$), the HQBS dip around the E^- subband top becomes a blue shifted broad valley, as shown by the dashed red lines in Figs. 4(b), (d) and 4(f). These HQBS dips are at $E = 0.985$, 0.990 , and 0.995 , respectively. The shift of the location of the HQBS is $\delta E = 0.005$ if the DFG potential is increased by $\delta V = 0.1$.

In order to demonstrate the possibility of forming a resonant state (RS) in a DFG system, we consider the system with a long FG distance, $L = 100$. The corresponding conductance is plotted as a function of energy shown in Fig. 5(a). When the gate voltage V is -0.2 (short dashed line), the conductance manifests a clear EQBS resonance dip at energy $E = 1.017$. However, for a positive gate voltage $V = 0.2$ (solid line) the conductance displays a more complicated structure. There is a broad resonance leading to a valley structure around $E = 0.9838$ corresponding to a HQBS with a binding energy

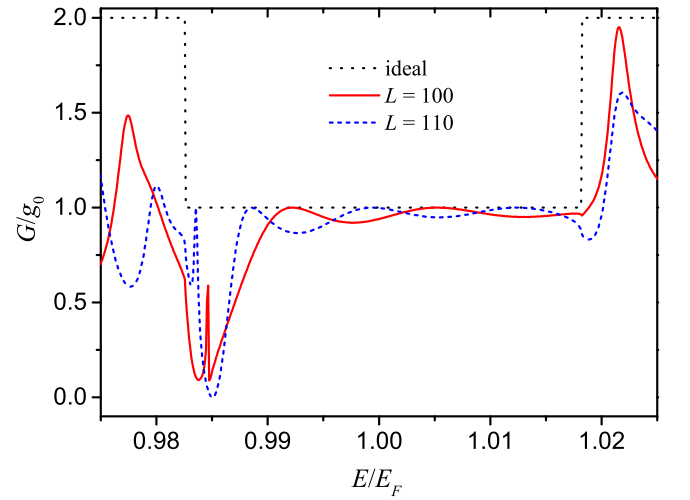


FIG. 6. (Color online) Conductance as a function of energy for a DFG system with $L = 100$ (solid) and 110 (dash). $\alpha = 0.2$, $\beta = 0.1$, and $gB = 0.02$.

approximately 0.0014 .

More importantly, when $V = 0.2$, a RS peak is found in the conductance around $E_{RS} = 0.985$ caused by multiple scattering between the two fingers leading to a resonant transmission. The corresponding energy $E_{RS}(n)$ can be estimated using an infinite quantum well model with a zero point energy measured from the subband top of the lower spin branch E_{0T}^- .

$$E_{RS}(n) = E_{0T}^- + \left(\frac{n\pi}{L}\right)^2, \quad (22)$$

in which $E_{0T}^- = 0.9824$, and hence we obtain $E_R(2) \sim 0.986$.

The probability densities shown in Figure 5(b)-(c) ($V = \pm 0.2$) are typical for resonances formed between finger gates. They are localized in the gate region, and due to the considerable length of the system ($L = 100$) the interference caused by the fingers is well visible as oscillations of the probabilities densities.

In order to provide further evidence that the peak at the energy $E = 0.985$, for gate potential $V = 0.2$ and distance $L = 100$ between the fingers (shown by red solid line in Fig. 5(a)) is a RS caused by multiple scattering we test its length dependence. We compare with results for $L = 110$ shown by a dashed blue curve in Fig. 6. The RS peak in the case of $L = 110$ is at $E = 0.984$ that is lower than for $L = 100$ and in accordance with what is to be expected. The dependence on the distance between the two fingers in the DFG system allows us to identify the sharp peaks in the conductance as a RS feature.

IV. CONCLUDING REMARKS

In conclusion, We have developed a model to investigate the interplay of the strong SO coupling and the Zee-

man effect, in which the lower spin branch contains a local band top in reciprocal space forming a SO-Z gap. We have demonstrated that this particular subband structure in SFG and DFG systems leads to interesting spin-resolved electronic transport properties.

In the absence of the Dresselhaus effect, the spin-split subband structure is symmetric with respect to the wave vector resulting in a degeneracy of the subband threshold. In this case, we identify the physical mechanisms responsible for the appearance for conductance mirror effect between the HQBS and EQBS in a SFG system. However, in a DFG system, the HQBS caused by a positive FG potential is strongly suppressed, but the EQBS feature remains significant.

In the presence of the Dresselhaus interaction, the subband structure becomes asymmetric with respect to the

wave vector. We successfully predict the binding energy of the real BS in the lower spin branch for both the SFG and the DFG systems. Especially, a RS can be found in a DFG system that is localized in the finger region due to multiple scattering. Our theoretical prediction of a formation of a BS and an RS mechanisms gives a hint for a design of a SO-Z based spin electronic device.

ACKNOWLEDGMENTS

This work was supported by the MOST in Taiwan through Contract No. 103-2112-M-239-001-MY3, the Icelandic Research and Instruments Funds, and the Research Fund of the University of Iceland.

-
- * cstang@nuu.edu.tw
- ¹ D. Loss and D. P. Divincenzo, Phys. Rev. A **57**, 120 (1998).
 - ² I. Žutić, J. Fabian, and S. Das Sarma, Rev. Mod. Phys. **76**, 323 (2004).
 - ³ S. A. Wolf, D. D. Awschalom, R. A. Buhrman, J. M. Daughton, S. von Molnár, M. L. Roukes, A. Y. Chtchelkanova, and D. M. Treger, Spintronics: A Spin-Based Electronics Vision for the Future, Science **294**, 1488 (2001).
 - ⁴ *Semiconductor Spintronics and Quantum Computation*, edited by D.D. Awschalom, N. Samarth, and D. Loss (Springer-Verlag, Berlin, 2002).
 - ⁵ D. D. Awschalom and M. E. Flatte, Nat. Phys. **3**, 153 (2007).
 - ⁶ S. Heedt, C. Morgan, K. Weis, D. E. Bürgler, R. Calarco, H. Hardtdegen, D. Grützmacher, and T. Schäpers, Nano Lett. **12**, 4437 (2012).
 - ⁷ E. I. Rashba, Sov. Phys. Solid State **2**, 1109 (1960); Y. A. Bychkov and E. I. Rashba, J. Phys. C **17**, 6039 (1984).
 - ⁸ R. Winkler, *Spin-Orbit Coupling Effects in Two-Dimensional Electron and Hole Systems*, Springer Tracts in Modern Physics Vol. 191 (Springer, Berlin, 2003).
 - ⁹ L. Meier, G. Salis, I. Shorubalko, E. Gini, S. Schon, and K. Enslin, Nat. Phys. **3**, 650 (2007).
 - ¹⁰ S. Bandyopadhyay and M. Cahay, Appl. Phys. Lett. **85**, 1814 (2004).
 - ¹¹ H. C. Koo, J. H. Kwon, J. H. Eom, J. Y. Chang, S. H. Han, and M. Johnson, Science **325**, 1515 (2009).
 - ¹² A. F. Sadreev and E. Ya. Sherman, Phys. Rev. B **88**, 115302 (2013).
 - ¹³ K. E. Nagaev and A. S. Goremykina, Phys. Rev. B **89**, 035436 (2014).
 - ¹⁴ C.-S. Tang, S.-T. Tseng, V. Gudmundsson, and S.-J. Cheng, J. Phys.: Cond. Mat. **27**, 085801 (2015).
 - ¹⁵ J. Nitta, T. Akazaki, H. Takayanagi, and T. Enoki, Phys. Rev. Lett. **78**, 1335 (1997).
 - ¹⁶ E. R. Mucciolo, C. Chamon, and C. M. Marcus, Phys. Rev. Lett. **89**, 146802 (2002); S. K. Watson, R. M. Potok, C. M. Marcus, and V. Umansky, *ibid.* **91**, 258301 (2003).
 - ¹⁷ A. Brataas, Y. Tserkovnyak, G. E. W. Bauer, and B. I. Halperin, Phys. Rev. B **66**, 60404 (2002).
 - ¹⁸ P. Zhang, Q. K. Xue, and X. C. Xie, Phys. Rev. Lett. **91**, 196602 (2003).
 - ¹⁹ B. G. Wang, J. Wang, and H. Guo, Phys. Rev. B **67**, 092408 (2003).
 - ²⁰ L. Serra, D. Sánchez, and Rosa López, Phys. Rev. B **72**, 235309 (2005).
 - ²¹ M. Scheid, D. Bercioux, and K. Richter, New J. Phys. **9**, 401 (2007).
 - ²² Q. F. Sun, H. Guo, and J. Wang, Phys. Rev. Lett. **90**, 258301 (2003).
 - ²³ W. Zeng, J. L. Wu, B. G. Wang, J. Wang, Q. F. Sun, and H. Guo, Phys. Rev. B **68**, 113306 (2003).
 - ²⁴ Y. V. Pershin, J. A. Nesteroff, and V. Privman, Phys. Rev. B **69**, 121306(R) (2004).
 - ²⁵ C. H. L. Quay, T. L. Hughes, J. A. Sulpizio, L. N. Pfeiffer, K.W. Baldwin, K.W. West, D. Goldhaber-Gordon, and R. de Picciotto, Nat. Phys. **6**, 336 (2010).
 - ²⁶ P. Zhang, Z.-L. Xiang, and F. Nori, Phys. Rev. B **89**, 115417 (2014).
 - ²⁷ G. Dresselhaus, Phys. Rev. **100**, 580 (1955).
 - ²⁸ C.-S. Tang, S. Y. Chang, and S. J. Cheng, Phys. Rev. B **86**, 125321 (2012).
 - ²⁹ D. Rainis and D. Loss, Phys. Rev. B **90**, 235415 (2014).
 - ³⁰ R. Landauer, Philos. Mag. **21**, 863 (1970).
 - ³¹ M. Büttiker, Phys. Rev. B **41**, 7906 (1990).